Journal of Power Sources 220 (2012) 217–227

Contents lists available at SciVerse ScienceDirect

Journal of Power Sources

journal homepage: www.elsevier.com/locate/jpowsour

Long term study of Cr evaporation and high temperature corrosion behaviour of Co coated ferritic steel for solid oxide fuel cell interconnects

J. Froitzheim*, S. Canovic, M. Nikumaa, R. Sachitanand, L.G. Johansson, J.E. Svensson

High Temperature Corrosion Centre (HTC), Chalmers University of Technology, Kemivägen 10, 41296 Göteborg, Sweden

HIGHLIGHTS

- Continuous Cr evaporation measurement for 3000 h.
- 640 nm Co coating showing no sign of degradation over 3000 h.
- Detailed TEM analysis of oxide scale/coating development from 15 s to 3000 h.

ARTICLE INFO

Article history:
Received 16 April 2012
Received in revised form
20 June 2012
Accepted 27 June 2012
Available online 7 August 2012

Keywords:
SOFC
Interconnect
Cr volatilization
TEM
Corrosion
Coating

ABSTRACT

The oxidation behaviour of the uncoated ferritic Fe-22Cr steel Sanergy HT is compared with an 640 nm Co coated version of the same material. The materials have been subject to corrosion and Cr volatilization measurements in air for up to 3000 h at 850 °C. Oxidation tests have been carried out both isothermal and discontinuously. The volatilization measurements were carried out using a recently developed denuder technique, which allows to quantify Cr evaporation in a time resolved manner. The oxidation process is studied from very initial phases (>15 s) to long term behaviour (3000 h). The formed oxide scales are analysed by XRD, SEM/EDX as well as TEM/EDX.

The results show that both materials form an oxide scale with an inner layer of Cr_2O_3 and a spinel layer on top. In the case of the uncoated material, the spinel layer is of $(Cr,Mn)_3O_4$ type while in the presence of a Co coating a $(Co,Mn,Fe)_3O_4$ is formed. The Cr evaporation measurements show that despite the fact that the Co coating is very thin (640 nm) it effectively blocks Cr evaporation for at least 3000 h. This is in line with TEM analysis showing that after 3000 h there is only a low Cr content in the outer oxide scale. This long term stability indicates the suitability of the coated material as solid oxide fuel cell (SOFC) interconnect.

1. Introduction

As solid oxide fuel cell (SOFC) operating temperatures have decreased in recent years, ferritic Fe–22 Cr steels have in most cases become the material of choice for interconnect applications. This type of material offers an attractive combination of relatively low production costs and a number of other advantages, such as e.g. ease of fabrication, good mechanical properties and excellent thermal matching with the other SOFC components. However, high temperature corrosion and chromium evaporation remain critical aspects that can have a severe impact on the lifetime of a SOFC stack. The trend towards lowering the operating temperatures of SOFC to as low as 600 °C reduces the problems with corrosion. However, even at such low temperatures substantial amounts of volatile $CrO_2(OH)_2$ can be formed [1,2]. Cathode poisoning due to volatile Cr species is well-known, and there are numerous publications discussing the mechanism by which Cr affects SOFC performance [3–8]. Several investigators have shown that $CrO_2(OH)_2$ is by far the dominant volatile Cr species under SOFC operating conditions [9–11].

In order to minimize Cr volatilization and to achieve a stable cell performance, the interconnect material has to be coated [12]. In recent years, numerous studies on such coatings have been published, out of which most studies focus on oxides of perovskites e.g. [13–16] or spinel type oxides e.g. [17–21], using various coating techniques such as PVD, thermal spraying or dip coating. Fewer publications discuss the application of metallic (mostly Co or Co based) coatings e.g. [22–25] Stanislowski et al. discussed not only Co but also Cu and Ni coatings [26]. Metallic coatings will usually oxidize under high temperature exposure and form an oxide cap

* Corresponding author. Tel.: +46 31 772 2858; fax: +46 31 772 2853.
E-mail address: Jan.froitzheim@chalmers.se (J. Froitzheim).

0378-7753/$ – see front matter © 2012 Elsevier B.V. All rights reserved.
http://dx.doi.org/10.1016/j.jpowsour.2012.06.092

Table 1
Nominal chemical composition of the steel Sanergy HT [30]. The Nb and Mo additions promote the formation of laves phase precipitates.

Element	Fe	Cr	C	Mn	Si	Al	Mo	Nb	Ti
Wt.%	Bal.	21.2	0.040	0.3	0.12	0.017	0.96	0.71	0.09

layer. Metallic coatings are expected to be attractive from an economic point of view since the raw materials are expected to be cheaper than rare earth based ceramics and high volume production processes like electroplating are feasible.

Commonly the coatings are evaluated in terms of their effect on cell performance while Cr volatilization is not measured directly. Only few studies [10,26–28] have directly quantified Cr volatilization. Such studies often rely on a transpiration technique where volatile Cr species are condensed in the cooler parts of the setup. The disadvantage of this method is that cumbersome cleaning is required to remove the deposited chromium, which is mainly in the trivalent state. This further requires disassembling the whole setup, with the consequence that only discontinuous measurements are possible and the time-resolution is limited. In the present study a denuder technique that was recently developed at Chalmers University of Technology has been employed [29]. This technique relies on a Na_2CO_3 getter which collects the gaseous Cr species at high temperature using a denuder tube. Hence, this method allows continuous isothermal operation and avoiding disassembling the equipment for every measurement.

2. Experimental

2.1. Materials

The samples are coupons of the ferritic Fe–22Cr steel Sanergy HT (commercial batch no 518053) with the dimensions $15 \times 15 \times 0.2$ mm^3. The steel has been manufactured by Sandvik AB, its composition is given in Table 1 [30]. In the study at hand, the uncoated material is compared with a Co coated version. The Co film (640 nm thick) was applied by Sandvik AB in a proprietary PVD process, more information on the coating process can be found in Ref. [31]. It is important to note that the samples were cut after the coating was applied, thus the edges are uncoated (this is discussed in more detail in Ref. [29]. Before exposure the samples were degreased and cleaned, both in acetone and ethanol, using an ultrasonic bath. The gravimetric measurements were made using a six decimal Sartorius balance.

2.2. Exposures

All experiments were carried out at 850 °C in a horizontal tubular silica glass reactor with an inner diameter of 46 mm (see Fig. 1). The experimental atmosphere was air with a humidity of 3% H_2O. This was prepared by leading the dried and filtered air first through a humidifier and then through a condenser set to a temperature of 24.4 °C. The experiments were carried out at a flow rate of 6000 ml min^{-1}. At this flow rate the gas has an average velocity of 27 cm s^{-1}, which corresponds to a regime where the evaporation rate is not flow dependent. A more detailed description can be found in Ref. [29]. The only differences between isothermal and discontinuous exposures were that in the latter case the samples were taken out for weighing and that the denuder tube was omitted. The given exposure time (15 s–3000 h) refers to the time in the furnace. This implies that during short term exposures the samples reached a temperature that was substantially lower than 850 °C. For the short term exposures (≤600 s) the samples were placed in an alumina boat in the hot zone of the tube furnace.

Downstream of the samples, the gas is fed through the silica glass denuder tube which has an inner diameter of 6 mm. The inside of the denuder tube is coated with Na_2CO_3, which reacts with the volatile Cr(VI) to Na_2CrO_4:

$$CrO_2(OH)_2(g) + Na_2CO_3(s) \rightarrow Na_2CrO_4(s) + H_2O(g) + CO_2(g)$$

The denuder tubes are replaced regularly and rinsed with MQ water. The Cr content of this solution is subsequently quantified by photospectrometry (Genesys 10UV, Thermo Scientific).

By comparing the weight loss of Cr_2O_3 pellets with the amount of Cr that was found after leaching the denuders, the collection efficiency of the denuder method was extensively tested and calculated to be 95 ± 5%. A more detailed description of the denuder technique can be found in Ref. [29].

2.3. Analysis

The SEM investigation was carried out using an FEI Quanta 200 FEG-SEM. For the TEM analysis an FEI Titan 80–300 TEM/STEM working at 300 kV was used. Both microscopes were equipped with an Oxford Inca EDX system that was used for compositional analysis. The TEM thin foils were prepared with an in-situ lift-out technique using an FEI Strata 235 DB FIB/SEM (focused ion beam/scanning electron microscopy) instrument.

X-ray diffraction measurements of the oxide layers formed on the steel coupons were carried out using a Siemens D5000 diffractometer with a grazing incidence set-up. Cu-Kα radiation was used and the measurements were carried out at a 3° angle of incidence.

3. Results

3.1. Oxidation and Cr evaporation

Fig. 2 shows the mass gains for the coated (triangle symbols) and uncoated version (square symbols) of Sanergy HT as a function of time. Both isothermal (open symbols) and discontinuous exposures (filled symbols) were carried out at 850 °C. The mass gain of the uncoated material matches reasonably well to parabolic kinetics ($k_p = \Delta m^2/t = 1.5 \times 10^{-13}$ g^{2}cm^{-4}s^{-1}). After 3000 h of exposure a mass gain of approximately 1.2 mg cm^{-2} is recorded. The Co coated material exhibits a higher mass gain. This is mainly

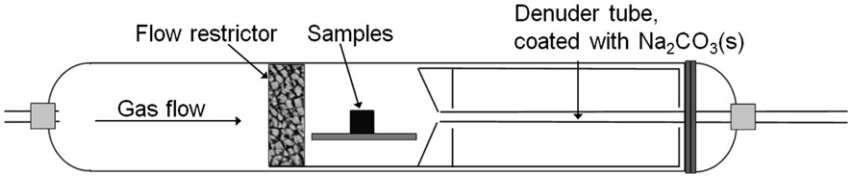

Fig. 1. Schematic drawing of the experimental setup.

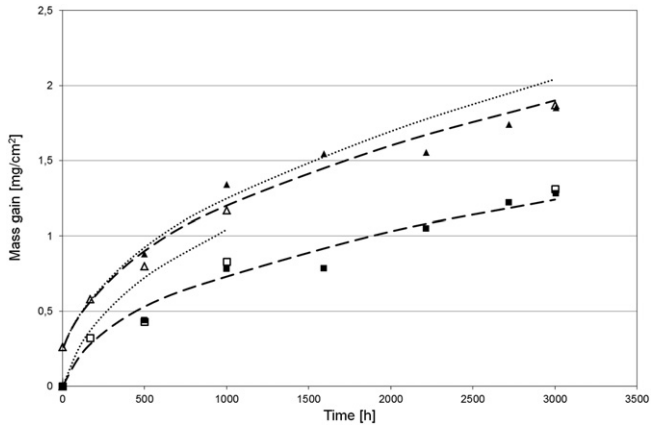

Fig. 2. Mass gain of 640 nm Co coated Sanergy HT (triangles) compared with uncoated Sanergy HT (squares) at 850 °C in air. The open symbols correspond to several isothermal exposures while the filled symbols represent discontinuous exposures. The dashed lines are manually fitted for illustration, the dotted lines are calculated by adding the calculated mass loss due to Cr evaporation to the measured mass gains.

attributed to the fast oxidation of Co in the initial phase. After 1 h a mass gain of 0.26 mg cm^{-2} is detected. This matches very well to an expected mass gain of 0.21 mg cm^{-2} if one assumes the oxidation of a 640 nm layer of metallic Co to Co_3O_4, because for the uncoated material a mass gain of 0.05 mg cm^{-2} is recorded. However, over time, the weight gain curves between uncoated and Co coated steel tend to diverge. This is mainly attributed to the higher chromium volatilization of the uncoated steel. Although the Co coated material also exhibits some Cr evaporation, the rate is much lower (see Fig. 3). The fact that the isothermal and discontinuous exposures fall on the same curve (within the expected scattering range) indicates that the scale has good stability under thermal cycling conditions.

The Cr evaporation from both materials is shown in Fig. 3. The uncoated material was measured for 1000 h while the Co coated material was measured for more than 3000 h. The Cr evaporation rate for the uncoated material is about one order of magnitude higher than for the Co coated material. The evaporation rate of the uncoated material decreases slightly with time. The Co coated material on the other hand exhibits an evaporation rate of approximately 3×10^{-7} kg m^{-2} h^{-1}, which is constant throughout the duration of the experiment.

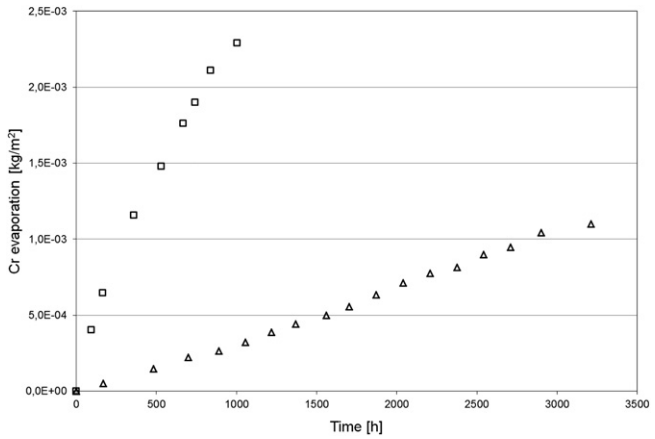

Fig. 3. Accumulated Cr evaporation as a function of time for Co coated Sanergy HT (triangles) and uncoated Sanergy HT (squares) at 850 °C (isothermal exposure) in air.

In order to compare the oxidation kinetics of the two materials, one has to compensate for the mass loss due to Cr evaporation by adding the corresponding mass loss to the measured mass gains. The mass loss is usually calculated as loss of Cr_2O_3. In this case a minor correction has to be made as it is expected that in both cases Cr evaporates from a spinel. The lost Cr^{3+} ion has to be replaced by a M^{2+} that needs to be oxidized to M^{3+} which requires $1/3O_2$ per Cr_2O_3 which is lost. The dotted lines in Fig. 2 show the theoretical mass gains if no evaporation had taken place. It can be seen that the curves approximately follow the same kinetics.

3.2. Analysis by XRD

X-ray diffractograms from unexposed Co coated Sanergy HT and from samples exposed for short times (0–3600 s) are shown in Fig. 4. The time refers to the time in the furnace which was set to 850 °C. However, the time at temperature is expected to be substantially lower if reached at all in case of the very short exposures. The XRD pattern of the unexposed sample shows peaks from the alloy substrate and from the metallic cobalt coating, which is hexagonally structured in the as coated state. The pattern remains largely unchanged after 15 s of heating, while 20 s of heating produce significant changes; the peaks from the hexagonally structured cobalt are no longer detected. Instead, a diffraction pattern from a face centered cubic structure is observed. This is related to a phase transition of the metallic cobalt from hcp to fcc. In addition there appears a halite structured phase proposed to be $Co_{1-x}O$ and a spinel structured phase proposed to be Co_3O_4. For exposures longer than 30 s (not shown) the metallic Co is absent in the diffractograms indicating rapid oxidation of Co. This also explains the decrease in intensity from the halite type oxide that oxidizes further to a spinel type oxide. The samples heated for 60, 600 and 3600 s generate similar XRD patterns, showing diffraction from two spinel oxides with slightly different cell volumes, one giving rise to strong diffraction while the other produces low intensity peaks.

3.3. Electron microscopy analysis of uncoated Sanergy HT

Fig. 5 shows a TEM bright field (BF) image of a cross-section of the oxide scale of uncoated Sanergy HT after 1 h of exposure. The oxide scale varies in thickness between 100 and 250 nm. The oxide grains are not clearly visible in the inner part of the oxide scale, probably because their diameter is smaller than the TEM lamella

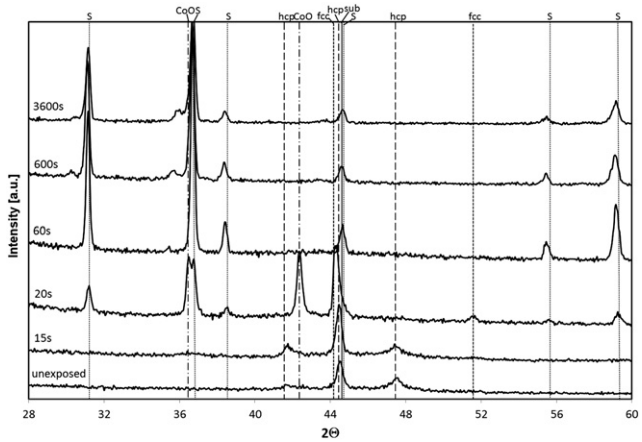

Fig. 4. Diffractograms of Co coated Sanergy HT exposed at 850 °C for various times. The expected 2Θ values for Co_3O_4 (S), CoO (CoO), hexagonal Co (hcp), cubic Co (fcc) and ferritic steel (sub) are marked.

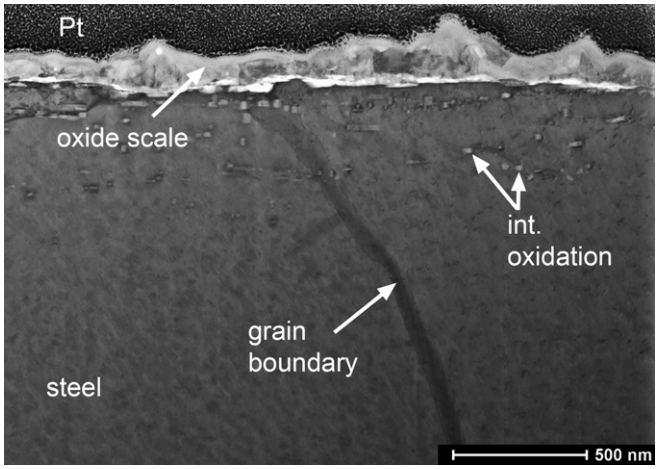

Fig. 5. TEM BF image of a cross-section of the oxide scale formed on the uncoated sample after 1 h exposure at 850 °C.

thickness (~100 nm) so they cannot be clearly resolved. The steel substrate exhibits a dark line representing an alloy grain boundary while the bright speckles beneath the oxide scale are due to internal oxidation of mainly Ti. Quantitative TEM/EDX maps of the oxide scale after 1 h of exposure are depicted in Fig. 6.

At this stage the oxide scale does not exhibit the clear separation between an inner Cr_2O_3 and an outer $(Cr,Mn)_3O_4$ scale as it is commonly observed [32,33]. Although the EDX maps (Fig. 6) show a trend towards this microstructure, it has not fully evolved yet. Instead it shows a rather chaotic, transient type of oxidation. It can be seen that the oxide scale is generally Cr rich, although the content varies from 50 to 90at.% (cations). The other main constituent of the oxide scale is Mn, which is present mainly in the outer part and in a continuous layer at the metal oxide interface. Substantial amounts of Fe and Ti are also present in the oxide scale in this initial stage.

The TEM BF image presented in Fig. 7 shows a cross-section of the oxide scale after 168 h of exposure. The total oxide scale thickness is approximately 3 μm. The oxide scale consists of two distinct layers; an inner Cr_2O_3 layer (2 μm) and an outer $(Cr,Mn)_3O_4$ layer (1–2 μm). The chromia layer consists of small equi-axed grains with a grain size of less than approximately 200 nm. In contrast, the spinel grains are much larger and elongated parallel to the oxide growth direction. A Mn-rich band was observed by EDX analysis (not shown) in the bottom part of the scale at the metal/oxide interface. This band indicates the presence of an inner Mn–Cr spinel oxide beneath the Cr_2O_3 layer, which will be discussed in more detail below. The precipitates in the steel substrate are Ti rich internal oxides. They also contain minor amounts of Al and Cr. At the metal/oxide interface, precipitates can be observed that appear dark in the BF image. These are expected to be of Laves phase type which is frequently reported in this type of material [32]. The composition of these precipitates, which are also located in the bulk of the material, is approximately (at.%) Fe 56%, Nb 28%, Cr 9%, Mo 6%. Below the Laves phase grains a steel grain boundary can be observed. However, neither feature seems to have a significant impact on the oxide scale morphology in their vicinity, although the spinel layer appears to be somewhat thicker in this area.

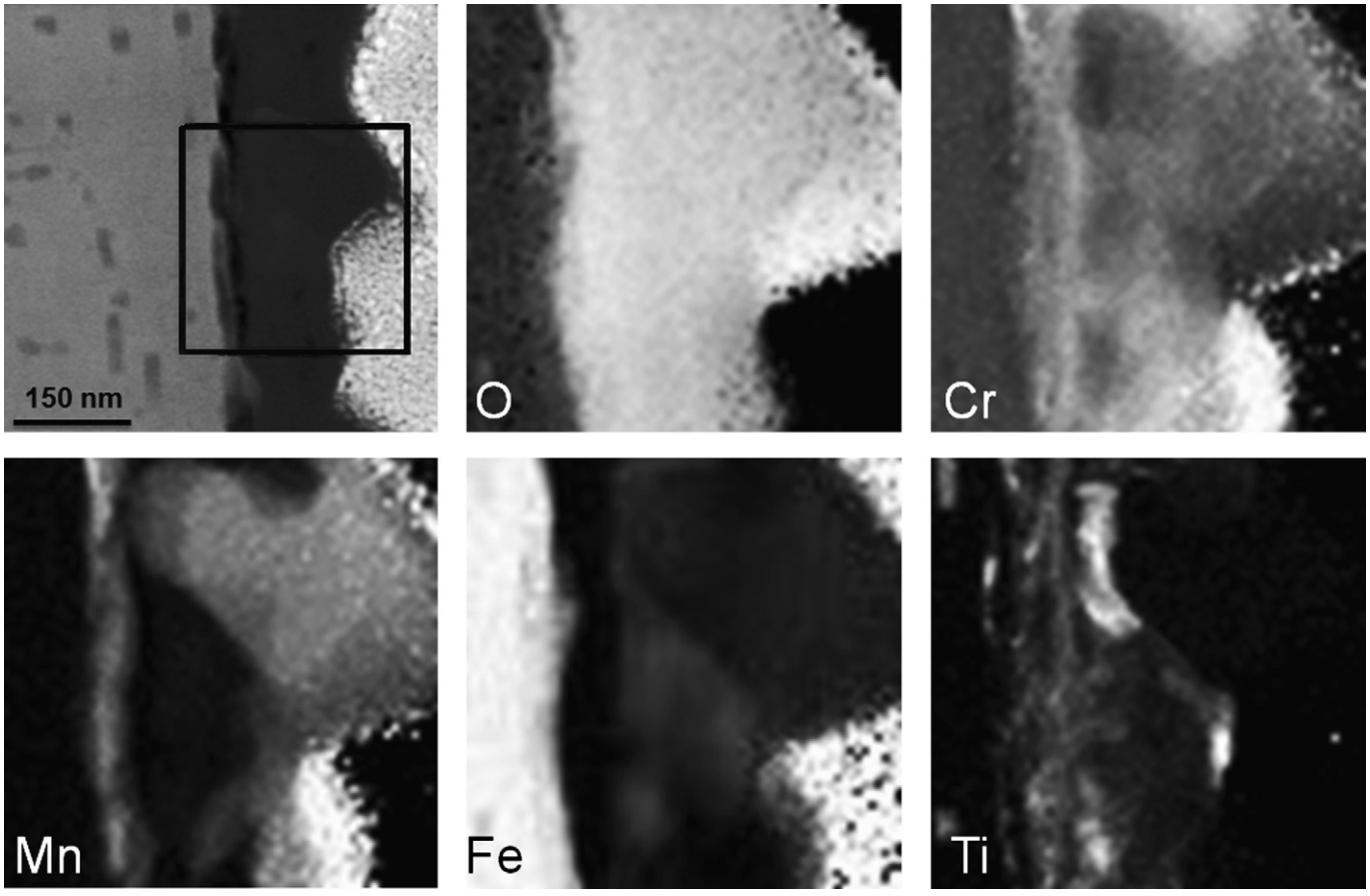

Fig. 6. Quantitative TEM/EDX maps of the oxide scale formed on the uncoated sample after 1 h exposure. (90° rotated view).

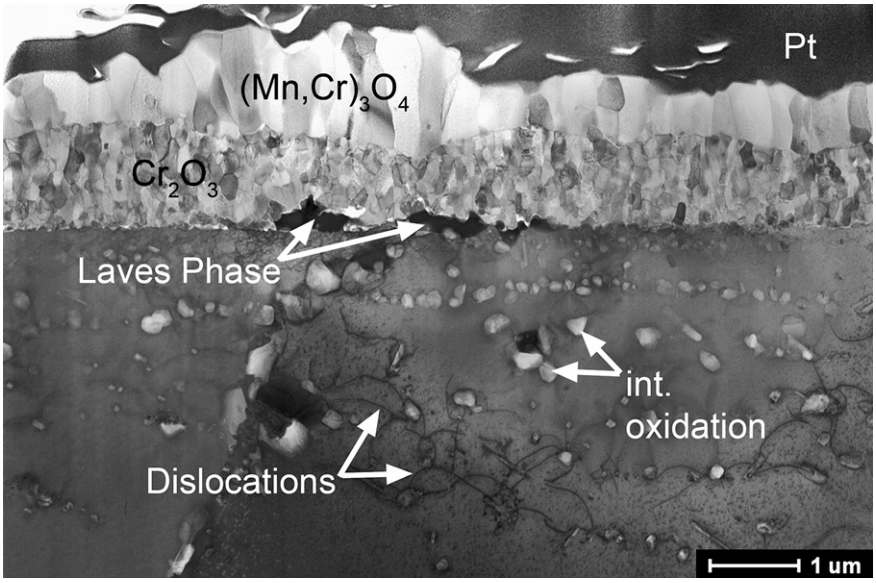

Fig. 7. TEM BF image of a cross-section of the oxide scale formed on the uncoated sample after 168 h exposure at 850 °C.

The scale morphology of the uncoated sample after 3000 h can be seen in Fig. 8. The oxide scale thickness is approximately 12–14 μm, the main part comprising of Cr_2O_3 (approximately 10–12 μm). Beneath the oxide scale fine precipitates can be found due to internal oxidation of minor alloying elements such as Ti or Al. In the steel, a number of Nb rich Laves phase type precipitates can be found. The EDX analysis of the steel matrix shows that the steel matrix is depleted in Cr (approximately 16at.% left) and Mn (below the detection limit). The depletion of Mn explains the absence of the inner Mn–Cr spinel oxide layer observed after 168 h (see discussion).

3.4. Electron microscopy analysis of Co coated Sanergy HT

The TEM analysis after 20 s oxidation (Fig. 9) confirms the findings of the XRD analysis. The oxidation time was sufficiently short to oxidize only the outer part of the Co layer while approximately half the original thickness is still present as metallic Co. At the steel/coating interface, a thin layer of native oxide is present. The grain size of the Co layer is approximately 500 nm with the grain boundaries being mainly perpendicular to the sample surface. The Co-oxide scale is very fine-grained and has a double layered stratigraphy. Based on the XRD results it is proposed that the outer layer (approximately 200 nm thick) is Co_3O_4, while the inner layer (50 nm) comprises of CoO. While the Co oxides are pure (within the accuracy of the EDX system), the metallic Co layer contains, closest to the steel, approximately 1.5at.% Fe and 1at.% Cr. Moreover, the steel closest to the surface contains 1–2at.% Co. This shows that interdiffusion of both Fe and Cr into the coating and Co into the steel has occurred during heating.

After 1 h of exposure (depicted in Fig. 10), the Co layer is completely oxidized. The oxide layer consists of an outer part that is

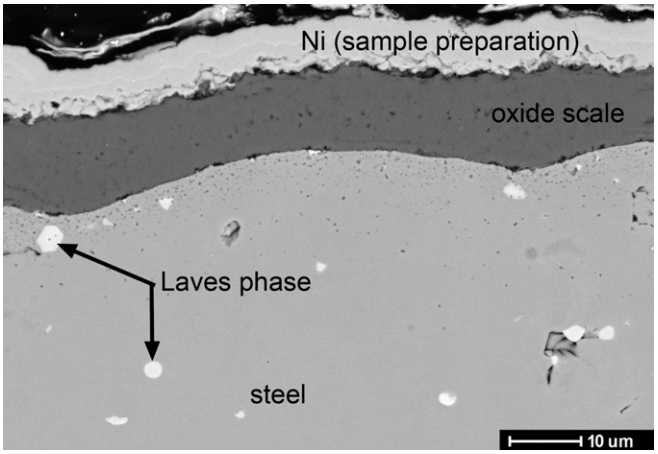

Fig. 8. SEM backscattered electron image of a cross-section of the oxide scale of uncoated Sanergy HT after 3000 h isothermal exposure at 850 °C.

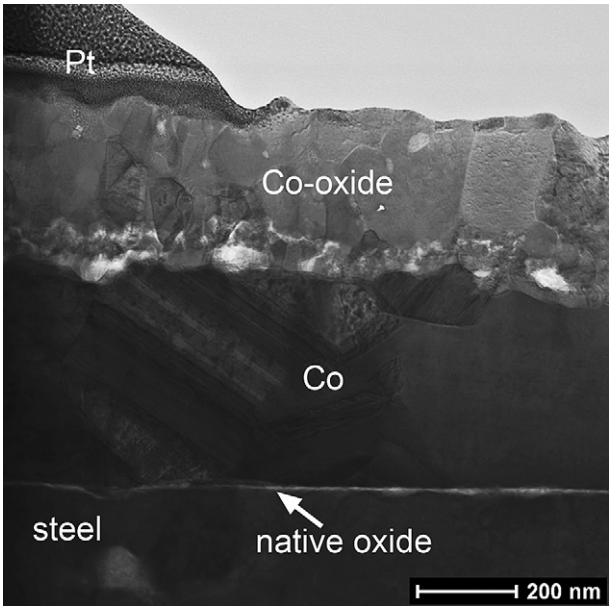

Fig. 9. TEM BF image of a cross-section of the oxide scale formed on the Co coated sample after 20 s exposure.

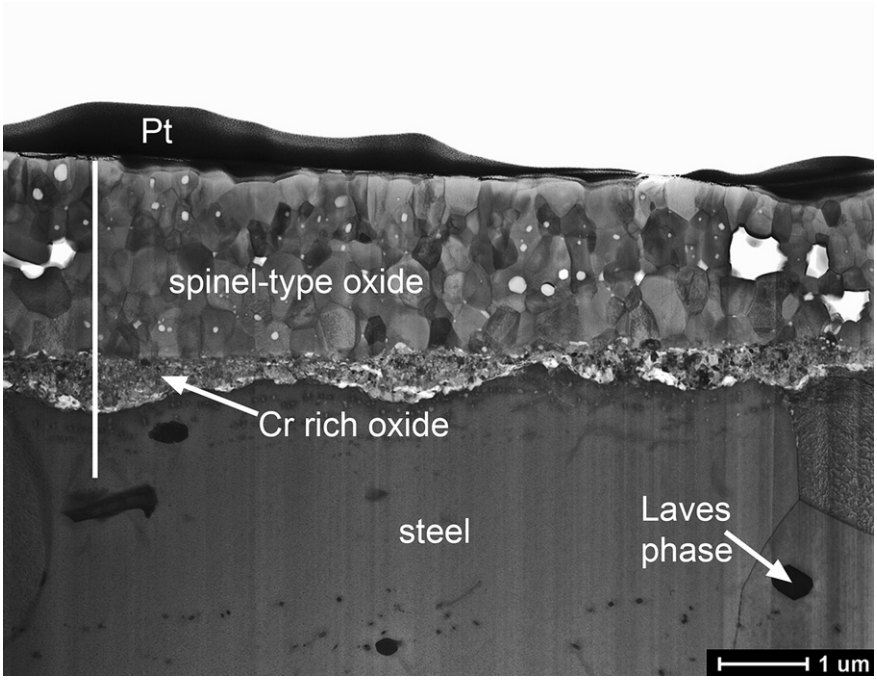

Fig. 10. TEM BF image of a cross-section of the oxide scale formed on the Co coated sample after 1 h exposure at 850 °C. The line marks the location of the EDX line scan presented in Fig. 10.

1.5 μm–2 μm thick and consists of large equiaxed grains (~500 nm in diameter). This part of the oxide scale also contains a number of pores indicating a fast growth of the oxide. The bottom part of the scale is fine-grained and has a thickness in the range 150–500 nm. The interface between these layers is perfectly straight and is considered to correspond to the former substrate/coating interface.

To further investigate the oxide scale morphology after 1 h oxidation, TEM/EDX quantitative mapping was carried out (see Fig. 12). The most apparent feature is that the outer (large-grained) scale consists of two layers that can hardly be distinguished in the TEM-BF image. Both parts seem to be spinel type oxides. However, the outermost part has a Co:Fe ratio that is close to 9:1 while in the inner part of the large grained oxide the Co:Fe ratio is approximately 1:1. The sharp drop in Fe concentration in the spinel layer is also illustrated in the linescan presented in Fig. 11. The linescan starts in the steel substrate (left), continues through the inner part of the oxide, and ends just below the sample surface.

The Mn map in Fig. 12 shows that diffusion of Mn into the large grained oxide is on-going. However, after 1 h, the Mn content in the oxide grain centres is still very low. Instead Mn diffuses along the oxide grain boundaries. The amount of Mn seems to be higher in the inner (Fe rich) part of the spinel-type large grained oxide. Fig. 12

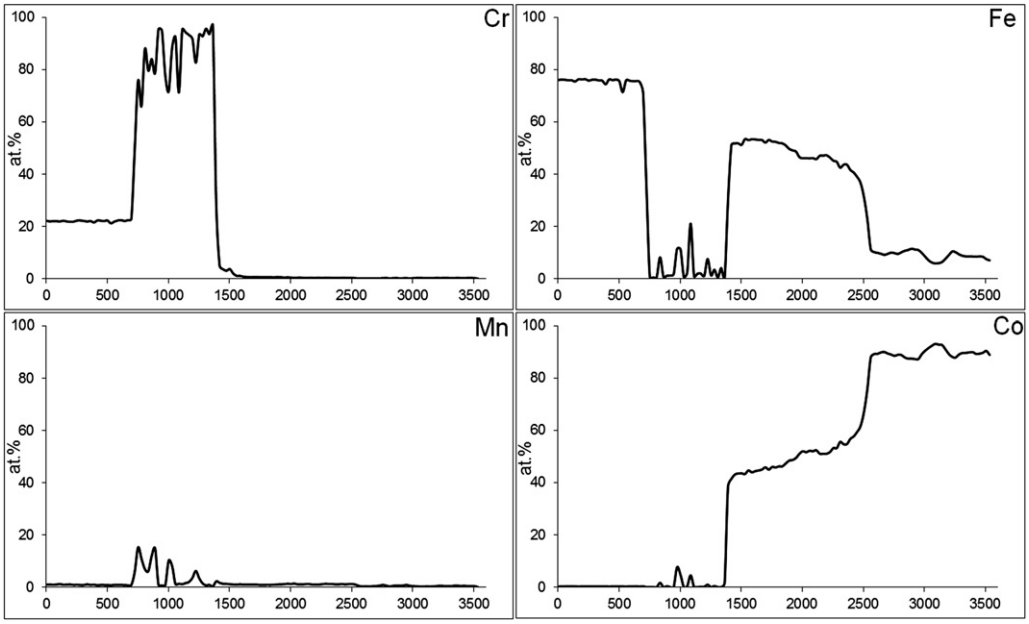

Fig. 11. EDX line scan from the steel (left) through the oxide scale of the coated sample after 1 h of exposure at 850 °C. See Fig. 9 for exact position.

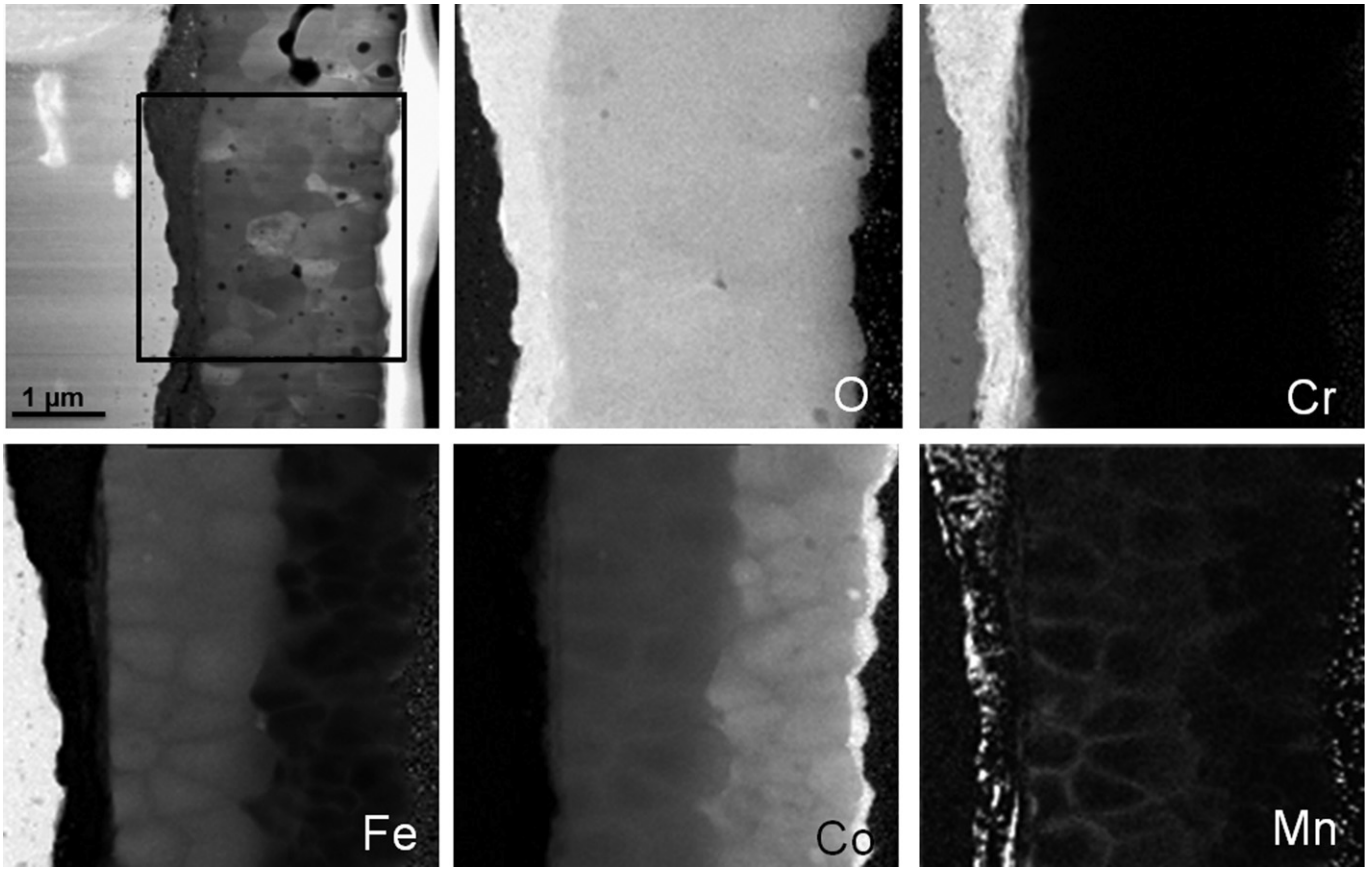

Fig. 12. Quantitative TEM/EDX maps of the oxide scale formed on the Co coated sample after 1 h exposure. (90° rotated view).

shows that the fine-grained bottom part of the scale consists mainly of Cr_2O_3. This part of the scale also includes substantial amounts of small (<100 nm) MnCr oxide particles proposed to consist of $(Mn,Cr)_3O_4$. Although they are present in the whole inner oxide scale, the highest concentration of these particles can be found at the metal/oxide interface.

Fig. 13 shows the oxide scale morphology of the Co coated sample after 168 h of exposure. The total oxide scale thickness is 4 µm. The outer scale which is 2.5 µm thick consists of large spinel grains with a diameter of up to 2 µm. Beneath the outer scale, an approximately 1.5 µm thick fine grained (grain size ~100 nm) Cr_2O_3 scale can be found. Compared to the 1 h exposure (see Fig. 10), the porosity of the outer layer seems to have decreased which indicates a healing mechanism. At the metal oxide interface, an approximately 300 nm thick layer of Mn rich spinel type oxide can be found (see Fig. 14). This appears to be the same type of oxide as observed on the uncoated steel in Fig. 7. However, it is more pronounced in the Co-coated material. Electron diffraction confirmed the spinel structure of this oxide [34]. TEM/EDX analysis revealed that the Cr_2O_3 scale is relatively pure (>98at.% cations) and that the spinel layer has a more uniform composition than after 1 h. The inner half of the spinel exhibits a rather constant Co:Fe ratio of 5:3 which gradually increases to the outer part (up to approximately 8:1 at the surface). Mn is almost evenly distributed in the outer spinel with an average concentration of approximately 10 cation%. Even though the centres of the largest spinel grains appear to contain less Mn.

A TEM BF image of a cross-section of the oxide scale after 3000 h of exposure is depicted in Fig. 15. The thickness of the outer spinel varies between 1.5 and 3 µm. Under the spinel layer, a 8–10 µm thick chromia layer can be found. The chromia grain size varies between approximately 100 and 300 nm, whereas the spinel grains are in the order of few µm. The TEM/EDX analysis shows that the Cr_2O_3 layer is pure (>99at.%), and that the composition of the spinel layer is constant over the layers thickness with a composition that matches $Co_{1.7}Mn_{0.75}Fe_{0.55}O_4$. Fig. 16 shows a EDX linescan taken

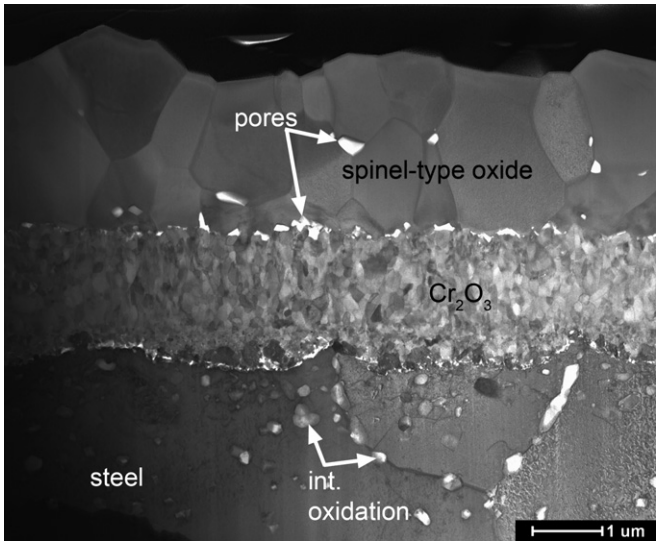

Fig. 13. TEM BF image of a cross-section of the oxide scale formed on the Co coated sample after 168 h exposure at 850 °C.

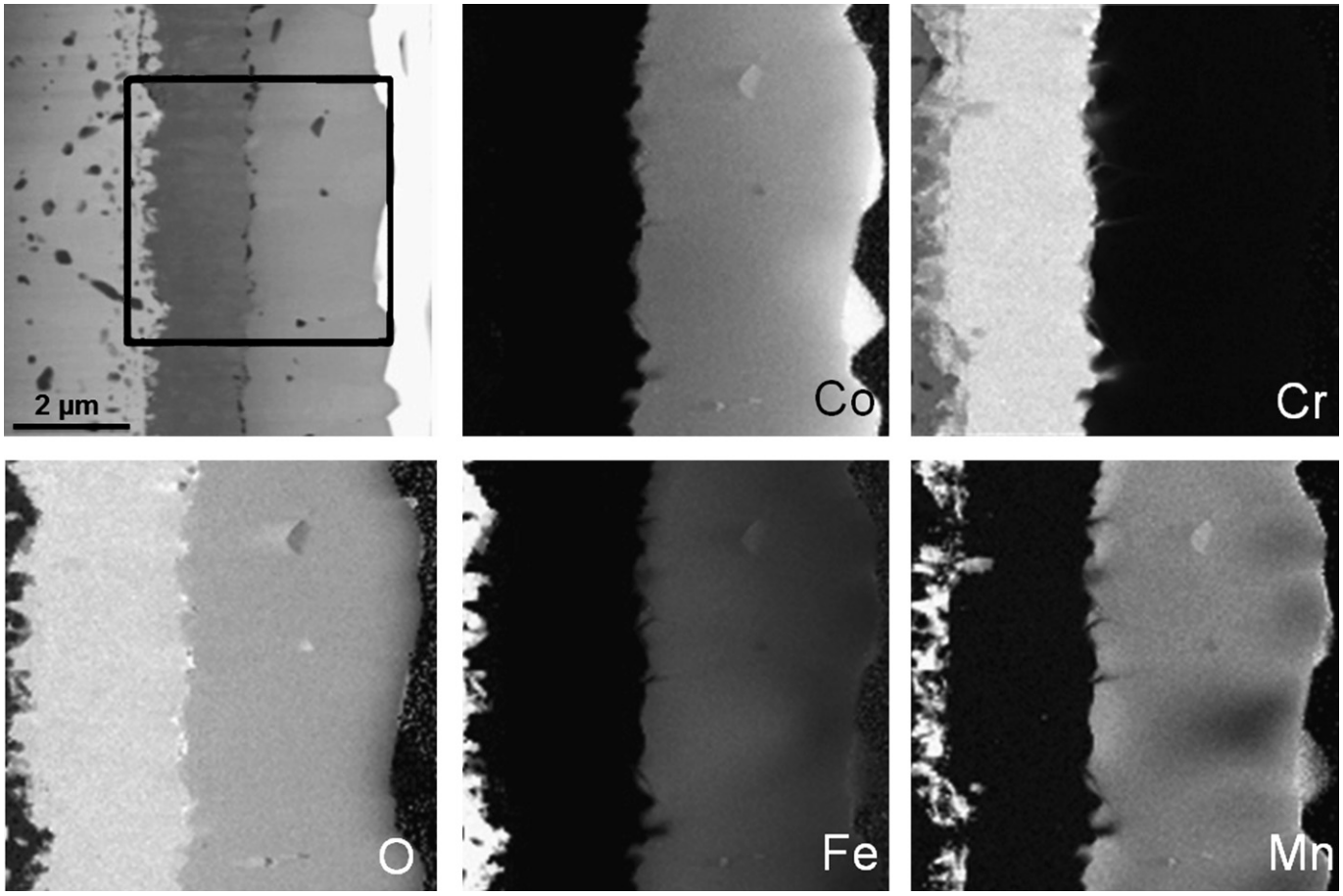

Fig. 14. Quantitative TEM/EDX maps of the oxide scale formed on the Co coated sample after 168 h exposure. (90° rotated view).

from the outermost part of the Cr_2O_3 layer (left) through the whole thickness of the $(Co,Mn,Fe)_3O_4$ layer. At this position the spinel layer is 1.8 μm thick and except for an area that is approximately 1.3 μm deep in the spinel the Cr content in the outer spinel layer is less than 1at.%. This together with the Cr evaporation data illustrates the effectiveness of the Co layer even after 3000 h of exposure.

4. Discussion

Although it is well-known that the chromium volatilization from stainless steels can be reduced substantially by Co coatings, only a few studies have quantified the effect. Kurokawa et al. [27] investigated 430 steel that was spray and dip coated with $MnCo_2O_4$ (oxide), and report a reduction of Cr evaporation for this material of a factor of 3 (dip coated) and 20 (spray coated) with coatings thickness of 35 μm and 20 μm respectively. The extensive investigation of different coatings by Stanislowski et al. [26] shows the high efficiency of a Co sputter coating of approximately 6 μm thickness. To the authors knowledge there is no previous work on sub-micron Co coatings and long-term investigations of Cr volatilization, as presented in the present paper, are lacking. As interdiffusion of substrate and coating elements is a widespread problem (observed e.g. in Ref. [26]), it is counterintuitive to expect long lifetimes for very thin coatings. However, Fig. 3 highlights the stability of the 640 nm Co coating over 3000 h with no trend pointing towards a degradation of the coating. This is confirmed by TEM/EDX analysis after 3000 h, which shows less than 1at.%Cr in the outer oxide layer. Nonetheless the diffusion of other steel alloying elements (Mn and Fe) into the coating is observed. The mass gain data of the discontinuous exposures presented in Fig. 2 also indicate a good stability against thermal cycling. However, more work employing harsh thermal cycling tests are required to verify this result.

Fig. 17 shows a schematic drawing of the chronology of the oxidation process for the Co coated material. The results show that the metallic Co layer oxidizes quickly during heating (in less than 30 s). In this short period of time a number of processes can be observed. First, and as long as a layer of metallic Co is present, the interdiffusion of Co into the substrate and Fe and Cr into the coating takes place. The presence of Fe in the Co layer promotes a phase transition from hexagonal Co into cubic Co that is taking place as illustrated by the phase diagram in Fig. 18.

Following this, once the Co layer is completely oxidized, no further diffusion of Fe into the coating is observed. This conclusion is based on the fact that the amounts (concentration × thickness) of Fe, measured by TEM/EDX in the spinel layer after 1, 168, and 3000 h, is not increasing over time. This behaviour of Fe is expected and is attributed to the selective oxidation of the more reactive alloy constituents.

After 1 h of exposure the Co coated sample has formed a 2 μm thick oxide layer due to the fast oxidation of the Co. The Cr rich layer that appears to be inward growing is mixed with Mn rich oxide particles, indicating that the exposure time was too short to produce the usually observed stratigraphy. The Mn content in the outer Co rich spinel grains is rather low and the EDX map in Fig. 12 clearly shows that Mn is diffusing outwards along the grain boundaries. Despite this, no substantial amounts of Mn have

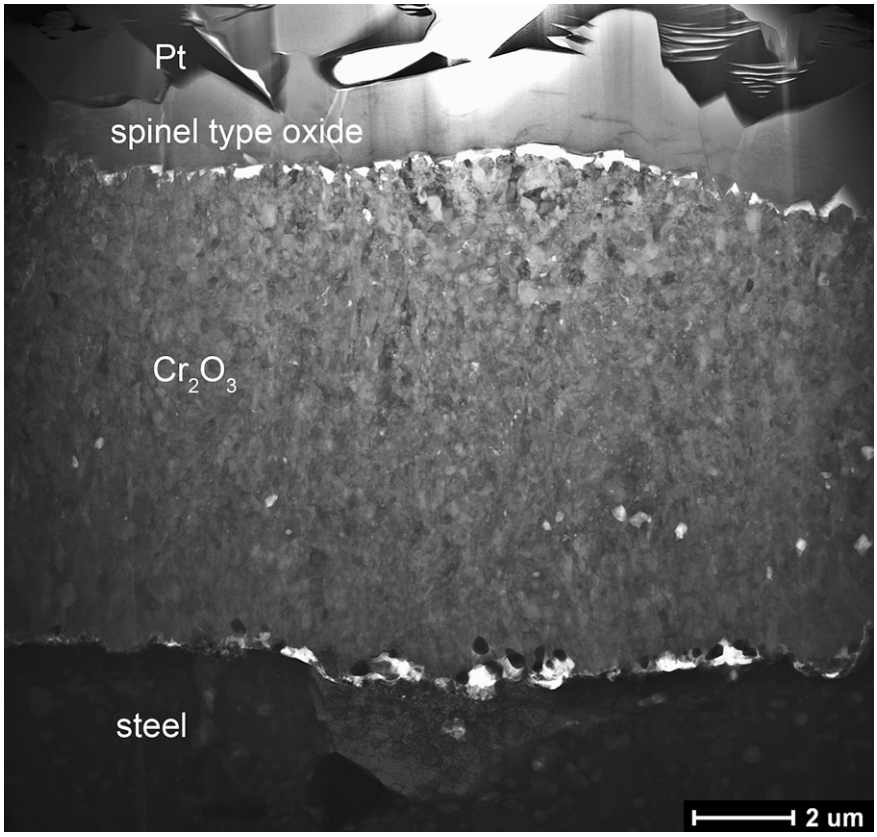

Fig. 15. TEM BF image of the a cross-section of the oxide scale formed on the Co coated sample after 3000 h exposure at 850 °C.

reached the surface after 1 h. Figs. 11 and 12 also show a step in Fe concentration within the spinel layer. It is suggested that this is related to the transition from Fe^{2+} to Fe^{3+}. According to Wagners oxidation theory, an oxygen activity gradient is present in the spinel layer. Thus, the mobile Fe^{2+} ions reach a position in the scale where the higher oxygen activity favours the oxidation from Fe^{2+} to less mobile Fe^{3+}.

After 168 h of exposure, the uncoated material exhibits the $Cr_2O_3/(Cr,Mn)_3O_4$ duplex layer scale that has been frequently observed for Sanergy HT and similar Fe–22Cr steels [35,36]. The

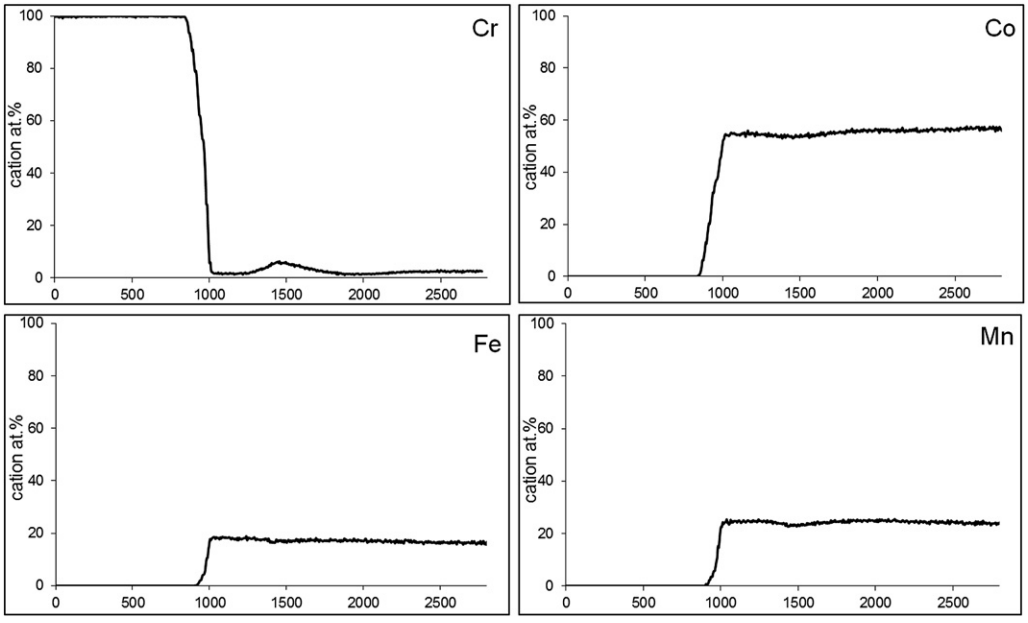

Fig. 16. EDX linescan through the outer part of the oxide scale of the Co coated sample after 3000 h of exposure at 850 °C.

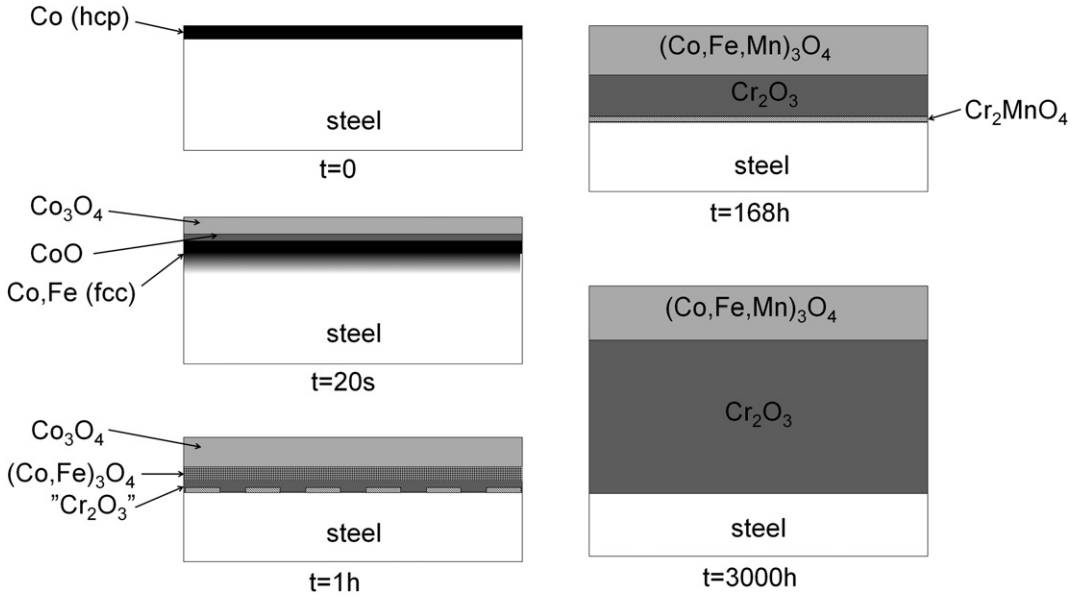

Fig. 17. Schematic drawing of the development of the oxide scale morphology of the Co coated sample.

scale thickness has grown from 200 nm (after 1 h) to 3 μm with a thickness ratio of approximately 1:1 between Cr_2O_3 and $(Cr,Mn)_3O_4$. In the Co coated case, the Cr_2O_3 layer has grown to a thickness of approximately 1.5 μm after 168 h which is about 3 times the thickness it exhibited after 1 h. In contrast, the Co rich spinel layer has only grown slightly in thickness. Thus the thickness ratio has changed from 1:5 after 1 h to 3:5 after 168 h. Inspection of the EDX maps shows that the concentration gradients observed after 1 h have evened out over time. The Co:Fe ratio is still higher closer to the surface, but instead of a stepwise increase there is a smooth gradient throughout the whole spinel layer thickness. Mn has enriched and also distributed more evenly in the spinel layer, and only the centres of the largest spinel grains exhibit lower than average Mn contents. It is concluded that the growth of the outer spinel layer can be mainly attributed to the incorporation of Mn supplied by the steel substrate.

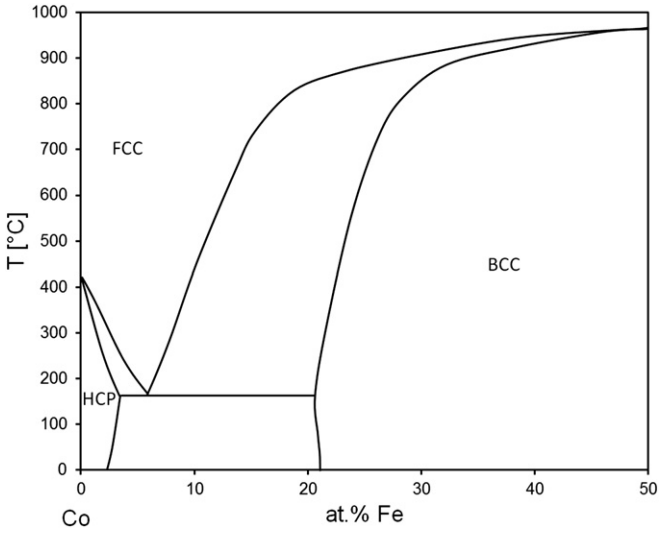

Fig. 18. Selected part of the Co–Fe phase diagram, based on calculations by Factsage [39].

In both the uncoated and the Co coated material, a Mn rich phase is observed at the metal/oxide interface (Fig. 14). This phase has been identified as cubic spinel by electron diffraction [34]. Although this inner spinel is more pronounced in the Co case, it is also clearly visible for the uncoated material. Such segregation of Mn rich oxide at the metal/oxide interface has been observed by other researchers [36]. The following mechanism is suggested to explain the presence of a spinel layer beneath the Cr_2O_3 layer: Since the solubility for Mn in Cr_2O_3 at low oxygen partial pressure is negligible [37,38], the oxidation of Mn forces the formation of $MnCr_2O_4$ at the metal/oxide interface.

This is caused by the fact that the Cr–Mn spinel phase is thermodynamically favoured compared to the presence of separate MnO/Cr_2O_3 phases [37,38]. Although Mn gradually diffuses outwards through the Cr_2O_3, the higher mobility of Mn in the steel compared to the mobility in Cr_2O_3 causes an accumulation of Mn at the metal/oxide interface. It is speculated that the presence of an outer Co-rich spinel reduces the diffusion of Mn through the scale and thus causes a larger accumulation of Mn at the metal/oxide interface.

After 3000 h of exposure, the steel is completely depleted in Mn, both in the coated and in the uncoated case. The inner spinel at the metal/oxide interface has also disappeared, which is in line with the discussion above. Due to the fact that the Mn supply from the steel has ceased at this stage, the composition of the outer spinel layer of the Co coated sample has completely evened out after 3000 h. However, this does not seem to have an effect on its Cr blocking properties (see Fig. 3). Thus a long term stability is expected that exceeds 3000 h. The outer spinel layer has almost the same thickness after 168 h (Fig. 13) and 3000 h (Fig. 15). Thus, the scale growth after longer exposures can be mainly attributed to a growth of the underlying Cr_2O_3 layer. This growth is expected to continue for longer exposure times, in this context it is important to note that 850 °C is a very demanding environment for a thin foil (0.2 mm) of Fe–22Cr steel. The uncoated material has reached a Cr concentration of only 16at.% after 3000 h, which fits very well to the calculated Cr loss due to the observed oxide scale thickness and measured Cr evaporation. Although no breakaway corrosion was observed, this level is considered to be close to the onset of breakaway corrosion [36]. Even though the Cr_2O_3 thickness for the Co coated material is

similar to that of the uncoated material, this material is expected to have a higher Cr content due to the lower Cr evaporation and the lack of a Cr rich spinel layer. This is in line with EDX measurements although it does not fit as well as for the uncoated case.

5. Conclusions

The comparison of uncoated Sanergy HT with a 640 nm Co coated version of Sanergy HT leads to the conclusion that the Co coated version possesses properties which makes it suitable for SOFC interconnect applications. The Cr evaporation measurements (Fig. 3) show that the evaporation rate is approximately one order of magnitude lower than for the uncoated material. It is important to note that the Co coated material exhibits a constant evaporation rate over the whole duration of the exposure (3000 h). The difference in Cr evaporation kinetics between both materials is due to a modification of the oxide scale by the Co coating. Both materials form an inner scale of Cr_2O_3 that is covered by a spinel layer. The uncoated material forms an outer $(Cr,Mn)_3O_4$ scale that gives rise to substantial Cr volatilization, while the coated steel forms a $(Co,Mn,Fe)_3O_4$ spinel on top of the Cr_2O_3 layer. The low rate of Cr evaporation for the Co coated material is because of the absence of Cr in the outer spinel layer. TEM/EDX analysis showed that this layer contains less than at.1% Cr even after 3000 h. The presence of Fe in the Co rich spinel layer can be understood by the investigation of very short exposures. After 20 s the Co layer is not yet completely oxidized. At this stage interdiffusion between the steel substrate and metallic Co is observed. Once the metallic Co layer is completely oxidized ($<$30 s), the Fe supply to the oxide ceases. Initially the Fe rich oxide is located in the innermost part of the spinel layer, and it takes substantially longer than a week to even out this concentration gradient.

Acknowledgements

This work was performed within the Swedish High Temperature Corrosion Centre. Sandvik Materials Technology is acknowledged for providing the samples. The financial support of the European Commission through the EU FP7 METSOFC project (Grant agreement no 211940), the Nordic Innovation Centre through the NaCoSOFC project and the national funding through the Swedish Energy Agency and the Swedish Research Council is gratefully acknowledged. Knut and Alice Wallenberg Foundation and the Swedish Research Council contributed to the financing of the TEM.

References

[1] H. Asteman, J.E. Svensson, M. Norell, L.G. Johansson, Oxidation of Metals 54 (2000) 11–26.
[2] H. Ravash, Chromium volatilization and oxidation of ferritic steels used as interconnects in solid oxide fuel cells, Master thesis, Chalmers University of Technology, Göteborg, Sweden, 2010.
[3] J.W. Fergus, International Journal of Hydrogen Energy 32 (2007) 3664–3671.
[4] N. Sakai, T. Horita, K. Yamaji, Y.P. Xiong, H. Kishimoto, M.E. Brito, H. Yokokawa, Solid State Ionics 177 (2006) 1933–1939.
[5] H. Yokokawa, T. Horita, N. Sakai, K. Yamaji, M.E. Brito, Y.P. Xiong, H. Kishimoto, Solid State Ionics 177 (2006) 3193–3198.
[6] T. Horita, Y.P. Xiong, H. Kishimoto, K. Yamaji, M.E. Brito, H. Yokokawa, Journal of the Electrochemical Society 157 (2010) B614–B620.
[7] T. Horita, Y. Xiong, M. Yoshinaga, H. Kishimoto, K. Yamaji, M.E. Brito, H. Yokokawa, Electrochemical and Solid-State Letters 12 (2009) B146–B149.
[8] G.Y. Lau, M.C. Tucker, C.P. Jacobson, S.J. Visco, S.H. Gleixner, L.C. DeJonghe, Journal of Power Sources 195 (2010) 7540–7547.
[9] B.B. Ebbinghaus, Combustion and Flame 93 (1993) 119–137.
[10] C. Gindorf, L. Singheiser, K. Hilpert, Journal of Physics and Chemistry of Solids 66 (2005) 384–387.
[11] E.J. Opila, D.L. Myers, N.S. Jacobson, I.M.B. Nielsen, D.F. Johnson, J.K. Olminsky, M.D. Allendorf, Journal of Physical Chemistry A 111 (2007) 1971–1980.
[12] N. Menzler, F. Tietz, S. Uhlenbruck, H. Buchkremer, D. Stöver, Journal of Materials Science 45 (2010) 3109–3135.
[13] A. Balland, P. Gannon, M. Deibert, S. Chevalier, G. Caboche, S. Fontana, Surface and Coatings Technology 203 (2009) 3291–3296.
[14] C.-L. Chu, J.-Y. Wang, S. Lee, International Journal of Hydrogen Energy 33 (2008) 2536–2546.
[15] Z. Yang, G.-G. Xia, G.D. Maupin, J.W. Stevenson, Journal of the Electrochemical Society 153 (2006) A1852–A1858.
[16] W.-J. Shong, C.-K. Liu, C.-Y. Chen, C.-C. Peng, H.-J. Tu, G.T.-K. Fey, R.-Y. Lee, H.-M. Kao, Materials Chemistry and Physics 127 (2011) 45–50.
[17] W. Qu, L. Jian, J.M. Hill, D.G. Ivey, Journal of Power Sources 153 (2006) 114–124.
[18] Z. Yang, G.-G. Xia, X.-H. Li, J.W. Stevenson, International Journal of Hydrogen Energy 32 (2007) 3648–3654.
[19] T. Uehara, N. Yasuda, M. Okamoto, Y. Baba, Journal of Power Sources 196 (2011) 7251–7256.
[20] J.P. Choi, K.S. Weil, Y.M. Chou, J.W. Stevenson, Z.G. Yang, International Journal of Hydrogen Energy 36 (2011) 4549–4556.
[21] B. Hua, Y.H. Kong, F.S. Lu, J.F. Zhang, J.A. Pu, J.A. Li, Chinese Science Bulletin 55 (2010) 3831–3837.
[22] W. Qu, L. Jian, D.G. Ivey, J.M. Hill, Journal of Power Sources 157 (2006) 335–350.
[23] J. Wu, C.D. Johnson, R.S. Gemmen, X. Liu, Journal of Power Sources 189 (2009) 1106–1113.
[24] C.M.C. Macauley, P. Gannon, M. Deibert, P. White, International Journal of Hydrogen Energy 36 (2011) 4540–4548.
[25] Q. Fu, F. Tietz, D. Sebold, E. Wessel, H.-P. Buchkremer, Corrosion Science 54 (2012) 68–76.
[26] M. Stanislowski, J. Froitzheim, L. Niewolak, W.J. Quadakkers, K. Hilpert, T. Markus, L. Singheiser, Journal of Power Sources 164 (2007) 578–589.
[27] H. Kurokawa, C.P. Jacobson, L.C. DeJonghe, S.J. Visco, Solid State Ionics 178 (2007) 287–296.
[28] M. Stanislowski, E. Wessel, K. Hilpert, T. Markus, L. Singheiser, Journal of the Electrochemical Society 154 (2007) A295–A306.
[29] J. Froitzheim, H. Ravash, E. Larsson, L.G. Johansson, J.E. Svensson, Journal of the Electrochemical Society 157 (2010) B1295.
[30] M. Schuisky, Analysis provided by Sandvik materials technology.
[31] U. Bexell, M. Olsson, M.W. Lundberg, High temperature oxidation of plastically deformed ferritic interconnect steel, in: S.C. Singhal, K. Eguchi (Eds.), Solid Oxide Fuel Cells, vol. 12, Electrochemical Society Inc., Pennington, 2011, pp. 2463–2470.
[32] J. Froitzheim, G.H. Meier, L. Niewolak, P.J. Ennis, H. Hattendorf, L. Singheiser, W.J. Quadakkers, Journal of Power Sources 178 (2008) 163–173.
[33] Z. Yang, P. Singh, J.W. Stevenson, G.G. Xia, Journal of Electrochemical Society 153 (2006).
[34] S. Canovic, J. Froitzheim, R. Sachitanand, M. Nikumaa, M. Halvarsson, J.E. Svensson, L.G. Johansson, Surface and Coatings Technology (2012).
[35] J. Hammer, S. Laney, R. Jackson, K. Coyne, F. Pettit, G. Meier, Oxidation of Metals 67 (2007) 1–38.
[36] P. Huczkowski, S. Ertl, J. Pirón-Abellán, N. Christiansen, T. Höfler, V. Shemet, L. Singheiser, W.J. Quadakkers, Materials at High Temperatures 22 (2006) 253–262.
[37] I.H. Jung, Solid State Ionics 177 (2006) 765–777.
[38] A. Naoumidis, H.A. Schulze, W. Jungen, P. Lersch, Journal of the European Ceramic Society 7 (1991) 55–63.
[39] FACTsage Software, GTT Technologies, Aachen, Germany.